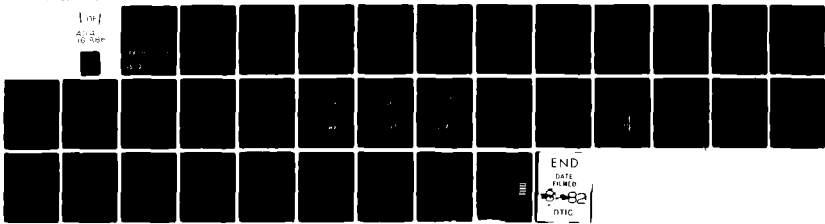


AD-A116 866 ARMY ARMAMENT RESEARCH AND DEVELOPMENT COMMAND ABERD--ETC F/8 19/4
NAVIER-STOKES COMPUTATIONS FOR CONVENTIONAL AND HOLLOW PROJECTI--ETC(U)
UNCLASSIFIED JUL 82 C J NIETUBICZ
ARBRL-MR-03184 S81-AD-F300 053 ML

1 of
4 of
10 Sep



12

AD A116866

AD

MEMORANDUM REPORT ARBRL-MR-03184

NAVIER-STOKES COMPUTATIONS FOR
CONVENTIONAL AND HOLLOW PROJECTILE
SHAPES AT TRANSONIC VELOCITIES

Charles J. Nietubicz

July 1982



US ARMY ARMAMENT RESEARCH AND DEVELOPMENT COMMAND
BALLISTIC RESEARCH LABORATORY
ABERDEEN PROVING GROUND, MARYLAND

Approved for public release; distribution unlimited.

DTIC FILE COPY

DTIC
ELECTE
JUL 13 1982

B

82 06 28 106

Destroy this report when it is no longer needed.
Do not return it to the originator.

Secondary distribution of this report by originating
or sponsoring activity is prohibited.

Additional copies of this report may be obtained
from the National Technical Information Service,
U.S. Department of Commerce, Springfield, Virginia
22161.

The findings in this report are not to be construed as
an official Department of the Army position, unless
so designated by other authorized documents.

*The use of trade names or manufacturers' names in this report
does not constitute indorsement of any commercial product.*

UNCLASSIFIED

SECURITY CLASSIFICATION OF THIS PAGE(When Data Entered)

cylinder and cylinder-boattail junctions as well as the movement of these shocks with varying free stream conditions. Surface pressure distributions and velocity profiles have been obtained and are compared with available experimental data for angle of attack, $\alpha = 0$. Additional results are shown for $\alpha = 2^\circ$, Mach = 0.96. The general geometry capability of the present method enables computations to be performed for many unique shapes such as hollow projectiles or ring airfoils. Internal and external pressure distributions are presented for a ring airfoil shape from Mach = 0.70 through Mach = 0.90.

2

UNCLASSIFIED

SECURITY CLASSIFICATION OF THIS PAGE(When Data Entered)

TABLE OF CONTENTS

	<u>Page</u>
LIST OF ILLUSTRATIONS.....	5
I. INTRODUCTION.....	7
II. GOVERNING EQUATIONS.....	8
A. Three-Dimensional Equations.....	8
B. Generalized Axisymmetric Equations.....	11
III. RESULTS.....	13
A. Secant-Ogive-Cylinder-Boattail, $\alpha = 0^\circ$	13
B. Secant-Ogive-Cylinder Boattail, $\alpha = 2^\circ$	14
C. Hollow Projectile, $\alpha = 0^\circ$	15
IV. SUMMARY.....	15
REFERENCES.....	28
LIST OF SYMBOLS.....	29
DISTRIBUTION LIST.....	31

Accession For	
NTIS SERIAL	<input checked="" type="checkbox"/>
DTIC	<input type="checkbox"/>
Unannounced	<input type="checkbox"/>
Justification	
By	
Distribution/	
Availability Codes	
Dist	Avail and/or Special
A	



3/4

LIST OF ILLUSTRATIONS

<u>Figure</u>		<u>Page</u>
1	Axisymmetric Body and Coordinate System.....	17
2	Mach Contours for SOCBT, $\alpha = 0^\circ$	18
	a. $M = 0.8$	18
	b. $M = 0.92$	18
	c. $M = 0.94$	19
	d. $M = 0.96$	19
	e. $M = 0.98$	20
	f. $M = 1.1$	20
3	Surface Pressure Coefficient for SOCBT, $\alpha = 0^\circ$	21
	a. $M = 0.94$	21
	b. $M = 0.96$	21
	c. $M = 0.98$	21
	d. $M = 1.1$	21
4	Wave Drag for SOCBT, $\alpha = 0^\circ$. Theory and Experiment.....	22
5	Comparison of Theoretical and Experimental Velocity Profiles for SOCBT.....	22
6	Windward and Leeward Surface Pressure Coefficients for SOCBT, $M = .96$, $\alpha = 2.0^\circ$	23
7	Mach Contours for SOCBT, $\alpha = 2.0^\circ$	23
8	3-D Velocity Profiles, $M = 0.96$, $\alpha = 2.0^\circ$	24
	a. $X/D = 4.76$	24
	b. $X/D = 5.05$	24
	c. $X/D = 5.59$	25
9	Inviscid Transonic Flow Over a Ring Airfoil Projectile, $\alpha = 0^\circ$	26
	a. $M = 0.4$	26
	b. $M = 0.7$	26
	c. $M = 0.8$	27
	d. $M = 0.9$	27

I. INTRODUCTION

The in-flight characteristics of an artillery shell are of major importance to the shell designer, ballisticians and ultimately the artillery field commander whose mission is deployment of timely and accurate fire power. The aerodynamic properties of artillery shell, such as pitching moment and Magnus moment are critical to the stability of shell which in turn significantly affect accuracy and time of flight. The capability to determine the aerodynamics of shell is required over a wide range of flight regimes since, depending on initial launch velocities, artillery shells are subject to subsonic, transonic, and supersonic flight. Projectile aerodynamics over these various flight regimes have been found, in some cases, to change by an order of magnitude. The solution techniques utilized must therefore be capable of computing these changes.

A concentrated theoretical and experimental research program has been ongoing at BRL in order to develop the predictive capabilities required for determining projectile aerodynamics. Supersonic computations using combined inviscid flow field and boundary layer techniques have been developed by Sturek¹, et al., for cone-cylinder and ogive-cylinder configurations. Recent results have been obtained in supersonic flow over a typical boattailed projectile by Schiff and Sturek² using modern computational techniques for solving the thin-layer Navier-Stokes equations.

Inviscid transonic computational results have been obtained by Reklis³, et al., for a secant-ogive-cylinder-boattail shape. The inviscid techniques give fair results for pitch plane aerodynamic coefficients at small angle of attack. The ability to compute the Magnus effect, however, relies on an accurate computation of the viscous boundary layer. Techniques which have been applied in supersonic flow for combining inviscid and boundary layer methods have not been fully established for transonic flow. These methods, which have shown good results for ogive-cylinders in supersonic flow at low angle of attack, are not accurate, however, in modeling the severe flow expansion in the vicinity of surface discontinuities such as those that occur at the cylinder-boattail junction.

-
1. Sturek, W. B., et al., "Computations of Magnus Effects for a Yawed, Spinning Body of Revolution," *AIAA Journal*, Vol. 16, No. 7, July 1978, pp. 687-692.
 2. Schiff, L. B., and Sturek, W. B., "Numerical Simulation of Steady Supersonic Flow Over Cone Ogive-Cylinder-Boattail Body," *AIAA Paper No. 80-0066*, 14-16 January 1980.
 3. Reklis, R. P., Sturek, W. B., and Bailey, F. L., "Computation of Transonic Flow Past Projectiles at Angle of Attack," *U.S. Army Ballistic Research Laboratory, ARRADCOM, Technical Report ARBRL-TR-02139*, February 1979. AD A069106.

The solution of the thin-layer Navier-Stokes equations, which allows for the simultaneous computation of the inviscid and viscous regions, eliminates the need for matching two different solutions. Additionally, since all three momentum equations are retained, the ability to compute in regions of separated flow is achieved. This paper describes the governing three-dimensional thin-layer Navier-Stokes equations used for computing flow over projectile shapes at angle of attack. Secondly, the generalized axisymmetric formulation used for computations at $\alpha = 0^\circ$ will be described. A description of the numerical algorithm and results will follow. Computational results and limited experimental data will be presented for a secant-ogive-cylinder-boattail projectile shape (SOCBT) at $\alpha = 0^\circ$. Additional computations have been obtained for the same projectile shape at $\alpha = 2^\circ$. Computational results will also be shown for a ring airfoil shape thus demonstrating the general geometry capability of the present numerical scheme.

II. GOVERNING EQUATIONS

The general three-dimensional thin-layer Navier-Stokes equations, used for all cases where $\alpha > 0^\circ$, are described in Section IIA. The thin-layer generalized axisymmetric equations, which are a special case in the 3-D equations, are described in Section IIB.

A. Three-Dimensional Equations

The transformed three-dimensional thin-layer Navier-Stokes equations in non-dimensional and strong conservation law form are written as⁴

$$\partial_\tau \hat{q} + \partial_\xi \hat{E} + \partial_\eta \hat{F} + \partial_\zeta \hat{G} = \text{Re}^{-1} \partial_\zeta \hat{S} \quad (1)$$

where general coordinate

- $\xi = \xi(x, y, z, t)$ - longitudinal coordinate
- $\eta = \eta(x, y, z, t)$ - circumferential coordinate
- $\zeta = \zeta(x, y, z, t)$ - near Normal coordinate
- $\tau = t$ - time

4. Pulliam, T. H., and Steger, J. L., "On Implicit Finite-Difference Simulations of Three-Dimensional Flow," *AIAA Journal*, Vol. 18, No. 2, February 1980, pp. 159-167.

are used and

$$\hat{q} = J^{-1} \begin{bmatrix} \rho \\ \rho u \\ \rho v \\ \rho w \\ e \end{bmatrix}$$

$$\hat{E} = J^{-1} \begin{bmatrix} \rho U \\ \rho u U + \xi_x p \\ \rho v U + \xi_y p \\ \rho w U + \xi_z p \\ (e+p)U - \xi_t p \end{bmatrix}$$

$$\hat{F} = J^{-1} \begin{bmatrix} \rho V \\ \rho u V + \eta_x p \\ \rho v V + \eta_y p \\ \rho w V + \eta_z p \\ (e+p)V - \eta_t p \end{bmatrix}$$

$$\hat{G} = J^{-1} \begin{bmatrix} \rho W \\ \rho u W + \zeta_x p \\ \rho v W + \zeta_y p \\ \rho w W + \zeta_z p \\ (e+p)W - \zeta_t p \end{bmatrix}$$

$$\hat{S} = J^{-1}$$

$$\begin{bmatrix} \mu(\zeta_x^2 + \zeta_y^2 + \zeta_z^2)u_\zeta + (\mu/3)(\zeta_x u_\zeta + \zeta_y v_\zeta + \zeta_z w_\zeta)\zeta_x \\ \mu(\zeta_x^2 + \zeta_y^2 + \zeta_z^2)v_\zeta + (\mu/3)(\zeta_x u_\zeta + \zeta_y v_\zeta + \zeta_z w_\zeta)\zeta_y \\ \mu(\zeta_x^2 + \zeta_y^2 + \zeta_z^2)w_\zeta + (\mu/3)(\zeta_x u_\zeta + \zeta_y v_\zeta + \zeta_z w_\zeta)\zeta_z \\ \{(\zeta_x^2 + \zeta_y^2 + \zeta_z^2)[0.5\mu(u^2 + v^2 + w^2)_\zeta \\ + \kappa Pr^{-1}(\gamma-1)^{-1}(a^2)_\zeta] \\ + (\mu/3)(\zeta_x u + \zeta_y v + \zeta_z w)(\zeta_x u_\zeta + \zeta_y v_\zeta + \zeta_z w_\zeta)\} \end{bmatrix}$$

The velocities in the ξ, η, ζ coordinates are

$$\left. \begin{aligned} U &= \xi_t + \xi_x u + \xi_y v + \xi_z w \\ V &= \eta_t + \eta_x u + \eta_y v + \eta_z w \\ W &= \zeta_t + \zeta_x u + \zeta_y v + \zeta_z w \end{aligned} \right\} \quad (2)$$

represent the contravariant velocity components.

The Cartesian velocity components (u, v, w) are retained as the dependent variables and are nondimensionalized with respect to a_∞ (the free stream speed of sound). The local pressure is determined using the relation

$$p = (\gamma - 1)[e - .5\rho(u^2 + v^2 + w^2)] \quad (3)$$

where γ is the ratio of specific heats, density (ρ), is referenced to ρ_∞ and total energy (e) to $\rho_\infty a_\infty^2$. The additional parameters are (κ) the coefficient of thermal conductivity, (μ) the dynamic viscosity, (Re) the Reynolds number, (Pr) the Prandtl number, and (λ) which through the Stokes hypothesis is $(-2/3)\mu$.

The metric terms of Equation (1) are defined from

$$\left. \begin{aligned} \xi_x &= J(y_\eta z_\zeta - y_\zeta z_\eta) & \eta_x &= J(z_\xi y_\zeta - y_\xi z_\zeta) \\ \xi_y &= J(z_\eta x_\zeta - x_\eta z_\zeta) & \eta_y &= J(x_\xi z_\zeta - x_\zeta z_\xi) \\ \xi_z &= J(x_\eta y_\zeta - y_\eta x_\zeta) & \eta_z &= J(y_\xi x_\zeta - x_\xi y_\zeta) \\ \zeta_x &= J(y_\xi z_\eta - z_\xi y_\eta) & \xi_t &= -x_t \xi_x - y_t \xi_y - z_t \xi_z \\ \zeta_y &= J(x_\eta z_\xi - x_\xi z_\eta) & \eta_t &= -x_t \eta_x - y_t \eta_y - z_t \eta_z \\ \zeta_z &= J(x_\xi y_\eta - y_\xi x_\eta) & \zeta_t &= -x_t \zeta_x - y_t \zeta_y - z_t \zeta_z \end{aligned} \right\} \quad (4)$$

and

$$J^{-1} = x_\xi y_\eta z_\zeta + x_\zeta y_\xi z_\eta + x_\eta y_\zeta z_\xi - x_\xi y_\zeta z_\eta - x_\eta y_\xi z_\zeta - x_\zeta y_\eta z_\xi$$

The "thin-layer" approximation⁴⁻⁷ used here requires that all body surfaces be mapped onto $\zeta = \text{constant}$ planes and $Re \gg 1$. Essentially, all the viscous (second derivative) terms in the coordinate directions (here taken as ξ and η) along the body surface are neglected while terms in the ζ or the near normal direction to the body are retained. This approximation is used because, due to computer speed and storage limitations, fine grid spacing can only be provided in one coordinate direction (usually taken as the near normal direction) and the grid spacing available in the other two directions is usually too coarse to resolve the viscous terms. For the type of problems currently under investigation, i.e., projectiles at low angles of attack, with no strong cross-flow separation, these approximations are considered valid.

B. Generalized Axisymmetric Equations.

The thin-layer generalized-axisymmetric equations are obtained from the three-dimensional equations by making use of two restrictions: (1) all body geometries are of an axisymmetric type; (2) the state variables and the contravariant velocities do not vary in the circumferential direction. In what follows, the $\partial_{\eta} \hat{F}$ term of Eq. (1) will be reduced to the source term of the generalized axisymmetric equations.

A sketch of a typical axisymmetric body is shown in Figure 1a. In order to determine the circumferential variation of typical flow and geometric parameters, we first establish correspondence between the inertial Cartesian coordinates (x,y,z) (to which the dependent variables are referenced), the natural inertial cylindrical coordinates (x,ϕ,R) , and the transformed variables (ξ,η,ζ) . The choice of the independent variables ξ, η, ζ is restricted, as shown in Figure 1c, insofar as η must vary as ϕ , i.e., $\phi = C\eta$ (where C is a constant). From the views shown in Figure 1, the relationship between the coordinate systems are observed to be

-
5. *Nietubicz, C. J., Pulliam, T. H., and Steger, J. L., "Numerical Solution of the Azimuthal-Invariant Thin-Layer Navier-Stokes Equations," U.S. Army Ballistic Research Laboratory, ARRADCOM, Technical Report ARBRL-TR-02227, March 1980. AD A085716.*
 6. *Steger, J. L., "Implicit Finite Difference Simulation of Flow About Arbitrary Geometries with Application to Airfoils," AIAA Paper No. 77-665, June 1977.*
 7. *Baldwin, B. S., and Lomax, H., "Thin Layer Approximation and Algebraic Model for Separated Turbulent Flows," AIAA Paper No. 78-257, January 1978.*

$$\left. \begin{aligned} \phi &= C\eta \\ x &= x(\xi, \zeta, \tau) \\ y &= R(\xi, \zeta, \tau) \sin \phi \\ z &= R(\xi, \zeta, \tau) \cos \phi \end{aligned} \right\} \quad (5)$$

where $\phi = \phi(\tau)$ and the Cartesian and cylindrical coordinates are related in the usual way. Note that x and R are general functions of only ξ , ζ , and τ .

Evaluating the metric terms given the above assumptions and substituting in Equation (1) the resulting unsteady thin-layer generalized axisymmetric equation⁵ can be written as

$$\partial_{\tau} \hat{q} + \partial_{\xi} \hat{E} + \partial_{\zeta} \hat{G} + \hat{H} = Re^{-1} \partial_{\zeta} \hat{S} \quad (6)$$

where

$$\hat{H} = J^{-1} \phi_{\eta} \begin{bmatrix} 0 \\ 0 \\ \rho V [R_{\xi} (U - \xi_{\tau}) + R_{\zeta} (W - \zeta_{\tau})] \\ -\rho V R \phi_{\eta} (V - \eta_{\tau}) - \rho / (R \phi_{\eta}) \\ 0 \end{bmatrix} \quad (7)$$

is the resultant source term which has replaced $\partial_{\eta} \hat{F}$ of Equation (1).

Equation (6) contains only two spatial derivatives but does retain all three momentum equations thus allowing a degree of generality over the standard axisymmetric equations. In particular, the circumferential velocity is not assumed to be zero allowing then computations for spinning projectiles or swirl flow to be accomplished.

The numerical algorithm used for both Equations (1) and (6) is a fully implicit, approximately factored finite difference scheme as analyzed by Beam and Warming⁸. Additional details of the numerical method, algorithm, and boundary conditions for each formulation can be found in References 4 and 5, respectively.

8. Beam, R., and Warming, R. F., "An Implicit Factored Scheme for the Compressible Navier-Stokes Equations," AIAA Paper No. 77-645, June 1977.

III. RESULTS

A series of computations has been obtained for a 3 caliber secant-ogive nose, 2 caliber cylinder, and 1 caliber, 7° boattail shape. The generalized axisymmetric formulation was used for all cases where $\alpha = 0^\circ$ and the 3-D Navier-Stokes Pulliam-Steger code was used for $\alpha > 0^\circ$. The results are presented in the form of contour plots, surface pressure distribution, and velocity profiles. Computations have been performed for a ring airfoil shape, the results of which show an interesting shock pattern being developed as a function of Mach number.

A. Secant-Ogive-Cylinder-Boattail, $\alpha = 0^\circ$.

A computational finite difference mesh of 78 longitudinal points by 50 normal points was used for these calculations. Grid points were clustered in the vicinity of the body surface discontinuities, which exist at the ogive-cylinder and cylinder-boattail junction. The grid points in the normal direction were exponentially stretched away from the surface with approximately 25 points located within the boundary layer. The Reynolds number for all cases was 0.72×10^6 based on body diameter and free stream velocity. The initial computation was for a free stream condition of Mach = 0.8. Additional runs were made by incrementing the free stream Mach number and using the previous converged solution as a starting condition. The results are first shown in the form of Mach contours in Figure 2. The regions of subsonic and supersonic flow are identified and the coalescence of the Mach lines to the right of the supersonic region represents the position of the shock. Initially at $M_\infty = 0.8$ (Figure 2a), only a small disturbance is felt in the free stream. As the Mach number is increased to 0.92 (Figure 2b), shocks are seen to occur on the cylinder and boattail. With a further increase in Mach number, the regions of supersonic flow have grown and the shocks have moved well downstream. A further increase in the free stream condition to $M_\infty = 1.1$ (Figure 2f) shows the beginning of a bow shock at the nose and expansion fans are evident at the surface discontinuities.

A more critical look at the computational results is shown in Figure 3 where the surface pressure coefficient, C_p , is shown as a function of axial position. The computational results are indicated by a solid line and the circles are experimental data obtained by Kayser⁹. Overall the comparisons show generally good agreement, however, some discrepancy is apparent near the expansions (decrease in C_p) and shocks (sharp increase in C_p) which indicates the need for additional mesh points in these areas. Additionally, the changing nature of the pressure distributions indicate that the varying shock

9. Kayser, L. D., and Whiton, F., "Surface Pressure Measurements on a Boattailed Projectile Shape at Transonic Speeds," BRL-MR to be published.

structure has been predicted quite well. An accurate computation of the pressure distribution is important since the integration of surface pressures is a major contributor in determining the aerodynamic coefficients. This is especially apparent in the transonic flight regime where the magnitude of the coefficients can change by as much as 100%. For the series of computations obtained from $M_\infty = 0.8$ through $M_\infty = 1.1$, the surface pressures were integrated to determine the aerodynamic wave drag. The results are shown in Figure 4 together with the available experimental data. Excellent agreement is shown for both the drag rise and magnitude of the wave drag in the critical Mach number regime.

The dynamic stability of shell is one area of concern when designing new shell or modifying existing ones. The Magnus moment, which affects the dynamic stability, is a viscous phenomenon occurring at $\alpha > 0^\circ$. Therefore an accurate representation of the viscous portion of the flow field is crucial to computing the Magnus moment. As an initial examination of the boundary layer in transonic flow, with its associated shock interaction, computations were performed at $M_\infty = 0.97$, $Re_D = 2.6 \times 10^6$ and $\alpha = 0^\circ$ for a similar projectile shape. A comparison of the computational velocity profiles with experimental data obtained by Danberg¹⁰ is shown in Figure 5. The results are shown for three axial stations in the vicinity of the boattail ($X/D = 5.3$). The profiles compare very well at $X/D = 5.05$ and 5.61 , which are stations approximately .3 in front of and behind the boattail corner. The profile at $X/D = 5.36$, which is in an area of severe expansion, is also considered quite good. The adequate resolution of the boundary layer which in this case includes a region of shock boundary layer interaction is very encouraging for future work in computing the Magnus effect.

B. Secant-Ogive-Cylinder-Boattail, $\alpha = 2^\circ$.

A new finite difference mesh consisting of 60 longitudinal points, 28 normal points, and 20 points in the circumferential direction was designed for computations at angle of attack. Clustering of the longitudinal points was maintained in the vicinity of the expansion similar to the $\alpha = 0^\circ$ cases. The computed leeward and windward pressure distributions are shown in Figure 6. The pressure on the ogive-nose is seen to be higher on the windward side, thus generating a positive or upward force on the projectile. The boattail region, however shows a reversal with the higher pressure now occurring on the leeward ray thus causing a negative or downward force. This resulting couple about the center of gravity is the main contributor to the critical aerodynamic behavior in the transonic regime. This effect can additionally be seen in the Mach contours of Figure 7. The asymmetry in the flow field is apparent

10. Danberg, J., *Wind tunnel data, to be published as a University of Delaware Report (Private communications).*

between the wind and lee side and more importantly the boattail shock is seen to be further aft on the wind side.

Velocity distributions obtained from the 3-D computations are shown in Figure 8 for three axial stations. The roll angle is located at the top of each profile with $\phi = 0^\circ$ and 180° corresponding to the lee and wind side, respectively. There are no experimental data for this case, however, the profiles do show a smooth variation with roll angle and become more full as the lee side is approached. Additionally, looking at the $\phi = 0^\circ$ plane for the three axial stations, the velocity is seen to increase near the boattail corner ($X/D = 5.0$) where the flow is expanding and then decrease on boattail ($X/D = 5.6$).

C. Hollow Projectile, $\alpha = 0^\circ$.

Of current interest in shell design is the utilization of hollow projectiles which have the characteristic of "flat" trajectories. A shape of this type, known as the ring airfoil, has been type classified and is currently used as an anti-riot device. In order to demonstrate the capability to compute flows about hollow projectile shapes of current Army interest, the generalized axisymmetric Navier-Stokes code was used for computations of a ring airfoil shape at $\alpha = 0^\circ$. A cross section of the actual shape is shown at the bottom of the C_p plot of Figure 9a. Inviscid results are presented in Figures 9a, b, c, and d for $M_\infty = 0.4, 0.7, 0.8,$ and 0.9 . In all cases the pressure distribution is plotted for the internal and external surfaces using a solid line and dashed line, respectively.

The critical pressure coefficient, C_p^* , is the value of the pressure coefficient at sonic velocity. The flow velocity in regions with pressure greater than C_p^* is subsonic and in regions where the pressure is less than C_p^* the flow is supersonic. For $M_\infty = 0.4$ (Figure 9a), all values of C_p are greater than C_p^* indicating the flow over both the internal and external surfaces is subsonic. However, as the Mach number is increased to 0.7, the upper surface is shown to develop supersonic flow and a shock wave while the internal flow remains subsonic. Increasing the Mach number still further to $M_\infty = 0.8$, the shock waves are now seen to exist on both the external and internal surfaces. A final solution at $M_\infty = 0.9$ shows that the shock wave has moved to the trailing edge indicating supersonic flow over most of the internal and external surfaces.

IV. SUMMARY

An implicit, finite difference technique has been used to solve the thin-layer Navier-Stokes equations. The three dimensional and generalized axisymmetric equations have been presented. Solutions are obtained for a secant ogive boattail and hollow projectile shape.

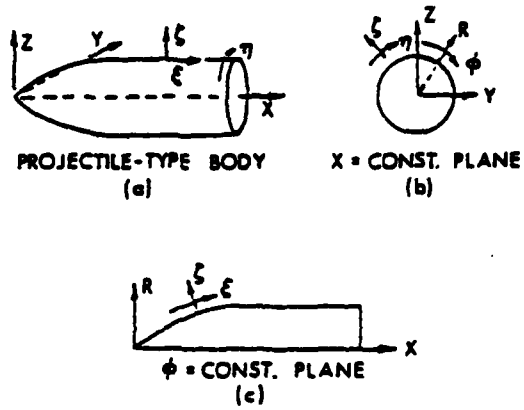
Comparisons of experimental and computed pressure distributions were obtained from Mach = 0.94 to 1.1. The comparisons indicated excellent agreement throughout the entire Mach number range. The movement of the shock position corresponding to changes in the free stream condition can be clearly seen from the Mach number contour plots.

The Navier-Stokes computations, which implicitly model the viscous and inviscid flow field, indicate excellent agreement with experimental velocity profile data for the $\alpha = 0$ case. This result is very encouraging since accurate prediction of the turbulent boundary layer development is critical to the determination of the Magnus force.

Results have been obtained for a projectile shape at $\alpha = 2.0$, Mach = 0.96. The general features of the flow field have been obtained. The Mach number contour plot shows the asymmetric shock pattern which exists on the boattail and pressure plots of wind versus lee side indicate the correct trends. A comparison of these results to experimental surface pressure and velocity profile data are required, however, to assess the accuracy of the three dimensional computations.

The general capability to compute internal flows has been demonstrated by solving the inviscid flow field about a ring airfoil projectile. Computations were obtained for Mach = 0.4 to 0.9. A significant change in the flow field has been found to occur throughout this regime. The Mach contours presented indicate regions of both subsonic flow and mixed subsonic/supersonic flow.

The results presented here provide a significant measure of confidence in using these new computational techniques for calculating projectile flow fields.



$$\begin{aligned} \phi &= C\eta \\ X &= X(\xi, \eta, \tau) \\ Y &= R(\xi, \eta, \tau) \sin \phi \\ Z &= R(\xi, \eta, \tau) \cos \phi \end{aligned}$$

Figure 1. Axisymmetric body and coordinate system

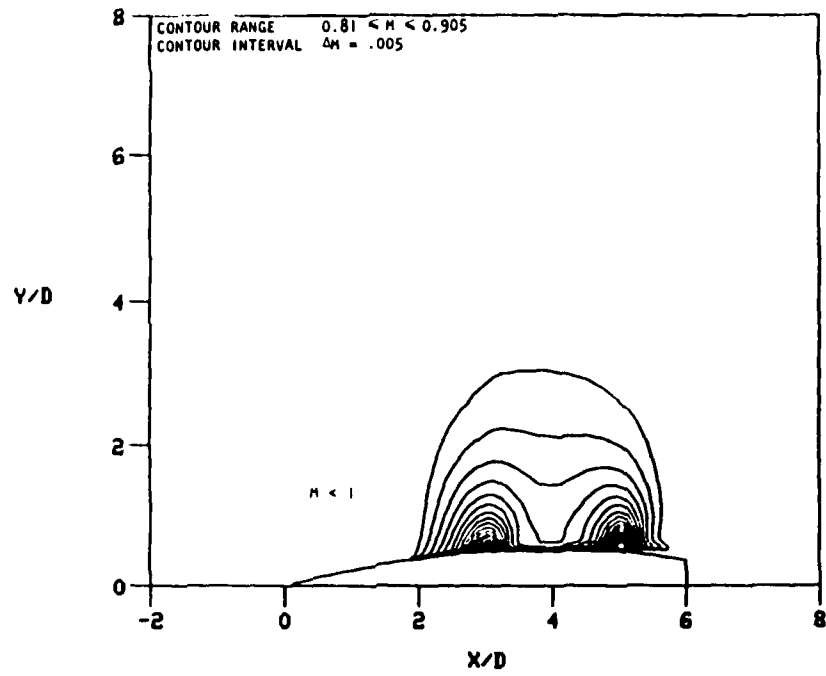


Figure 2a. Mach contours for SOCBT, $\alpha = 0^\circ$, $M = 0.8$

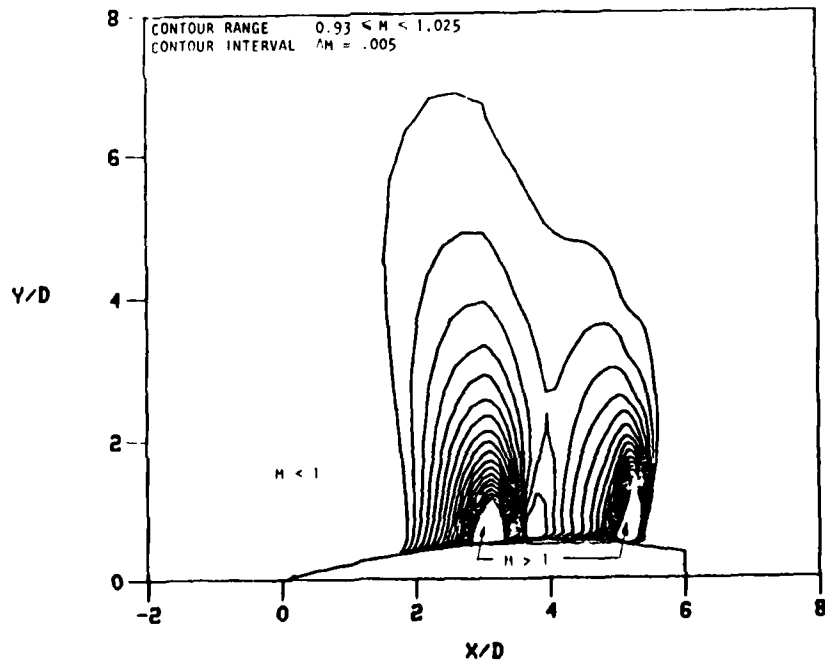


Figure 2b. Mach contours for SOCBT, $\alpha = 0^\circ$, $M = 0.92$

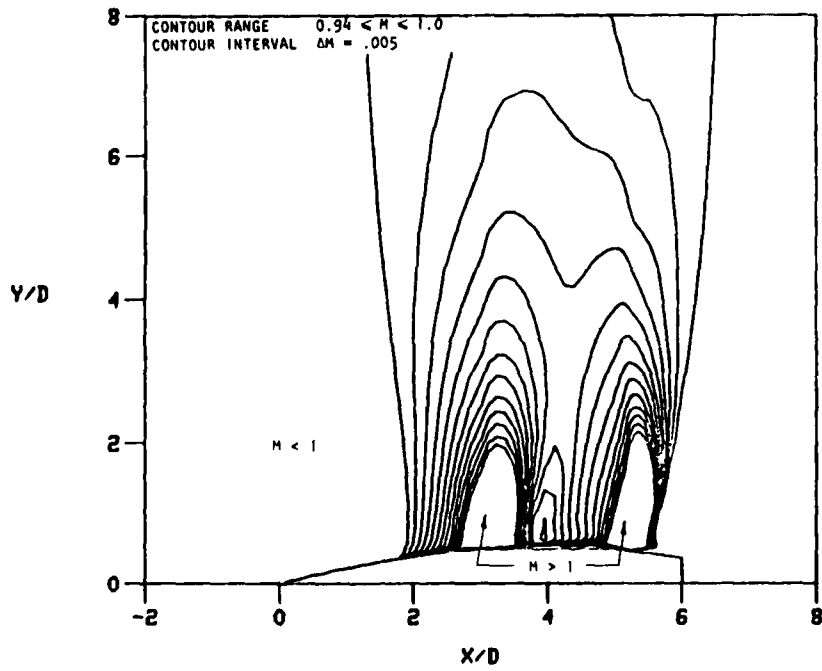


Figure 2c. Mach contours for SOCBT, $\alpha = 0^\circ$, $M = 0.94$

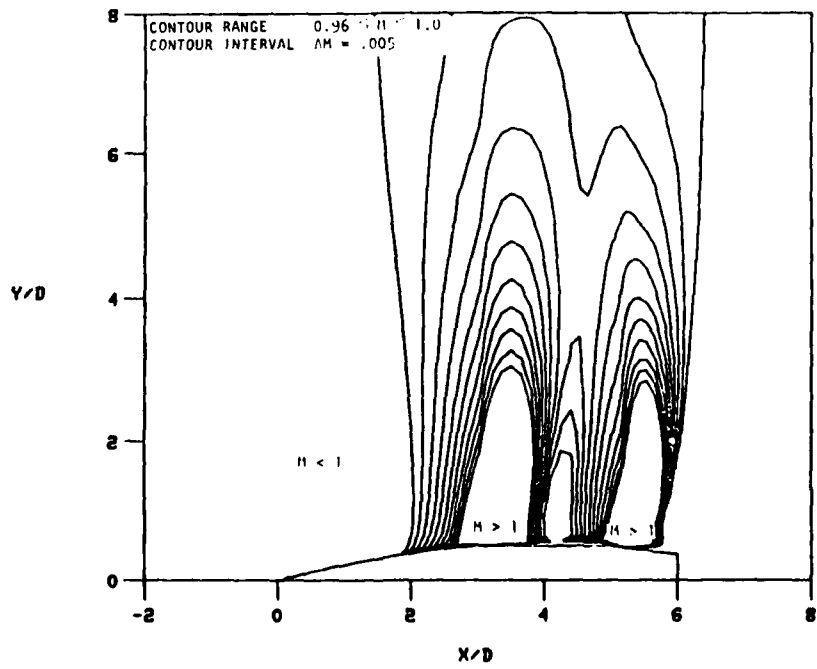


Figure 2d. Mach contours for SOCBT, $\alpha = 0^\circ$, $M = 0.96$

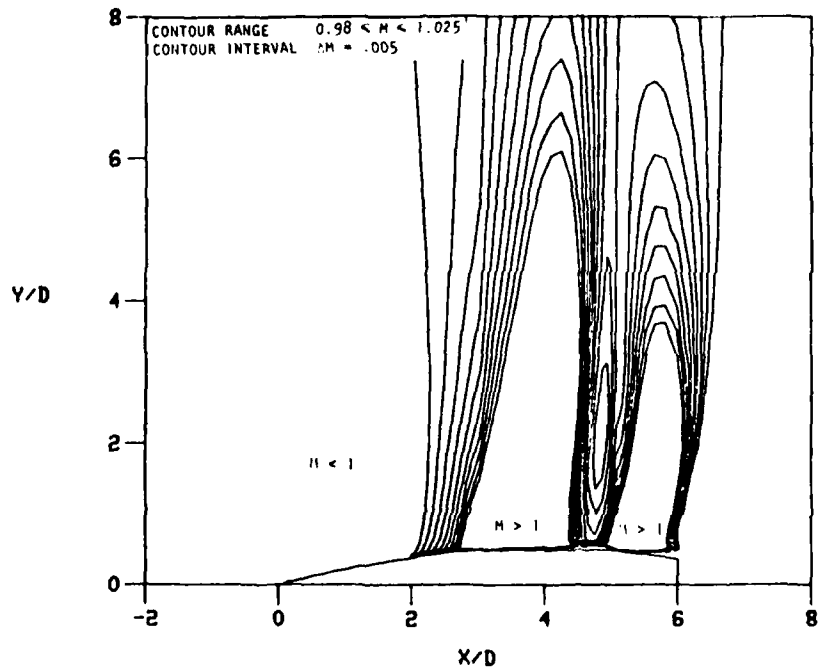


Figure 2e. Mach contours for SOCBT, $\alpha=0$, $M=0.98$

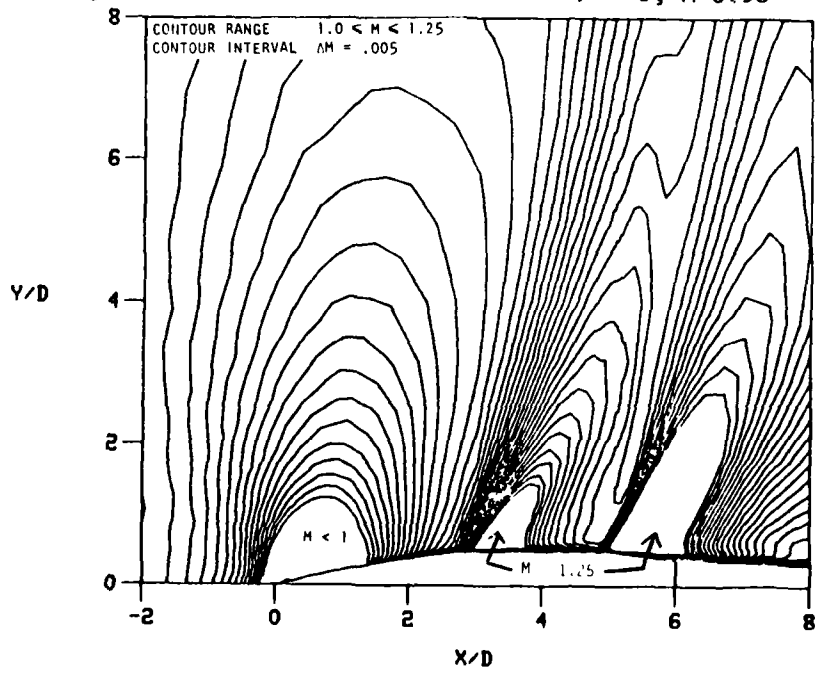


Figure 2f. Mach contours for SOCBT, $\alpha=0$, $N=1.1$

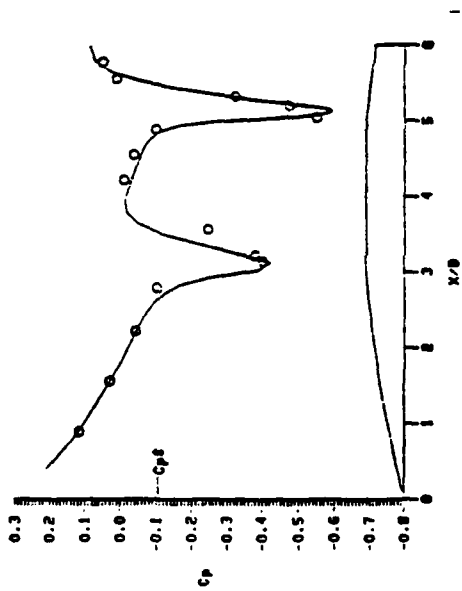


Figure 3a. Surface pressure coefficient for SOCBT, $\alpha = 0^\circ$, $M = 0.94$

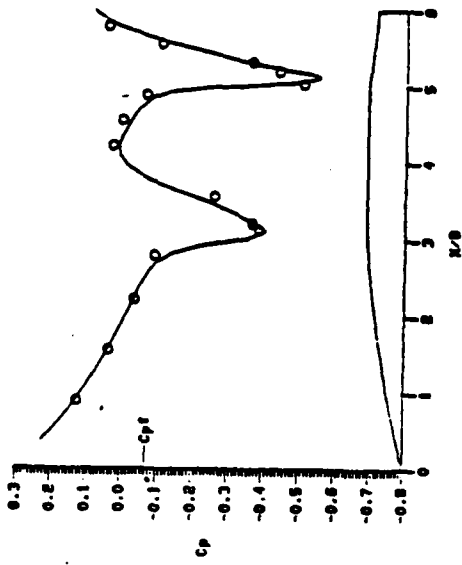


Figure 3b. Surface pressure coefficient for SOCBT, $\alpha = 0^\circ$, $M = 0.96$

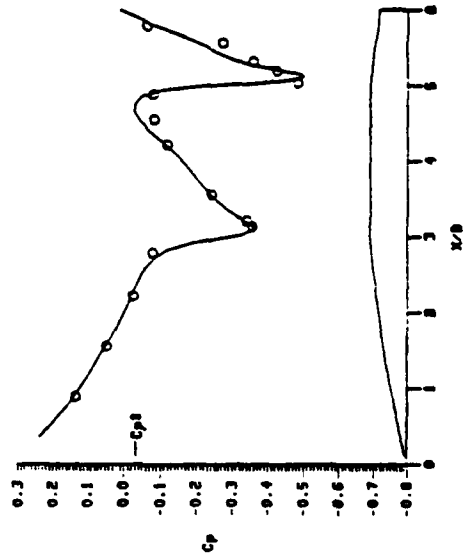


Figure 3c. Surface pressure coefficient for SOCBT, $\alpha = 0^\circ$, $M = 0.98$

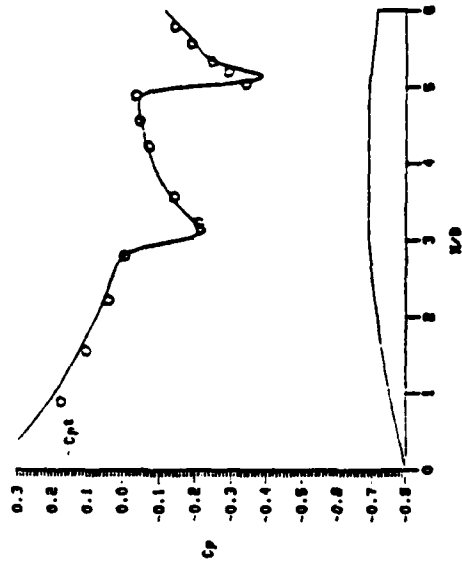


Figure 3d. Surface pressure coefficient for SOCBT, $\alpha = 0^\circ$, $M = 1.1$

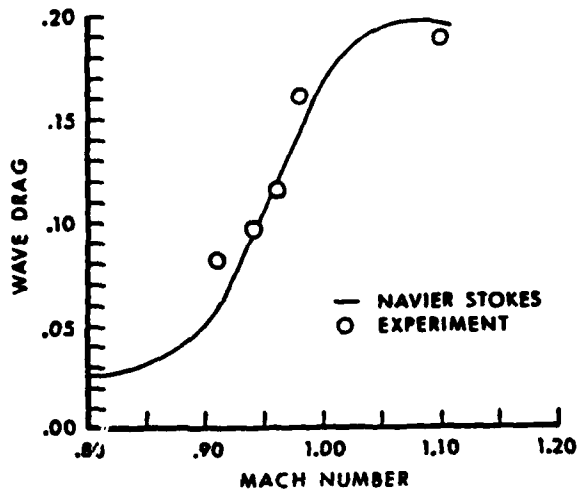


Figure 4. Wave drag for SOCBT, $\alpha = 0$. Theory and experiment.

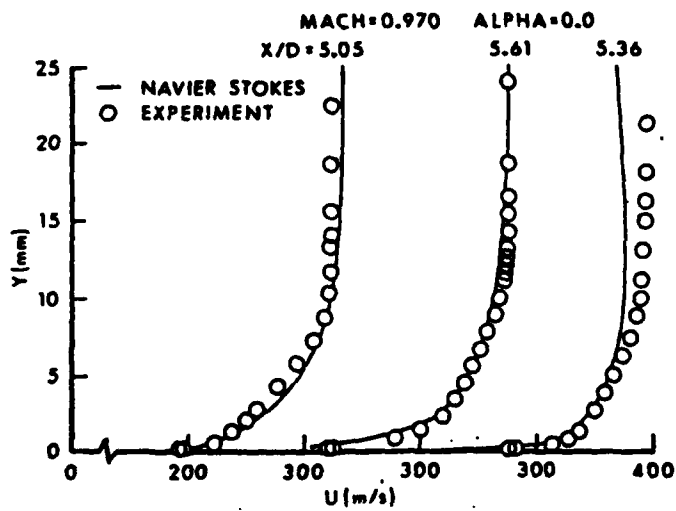


Figure 5. Comparison of theoretical and experimental velocity profiles for SOCBT.

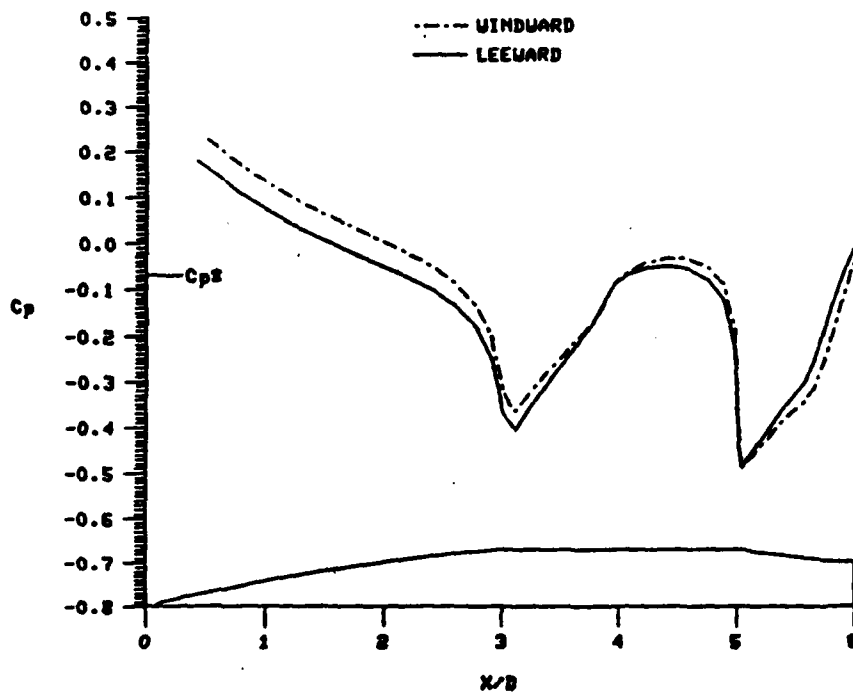


Figure 6. Windward and leeward surface pressure coefficient for SOCBT, $M = .96$, $\alpha = 2.0^\circ$

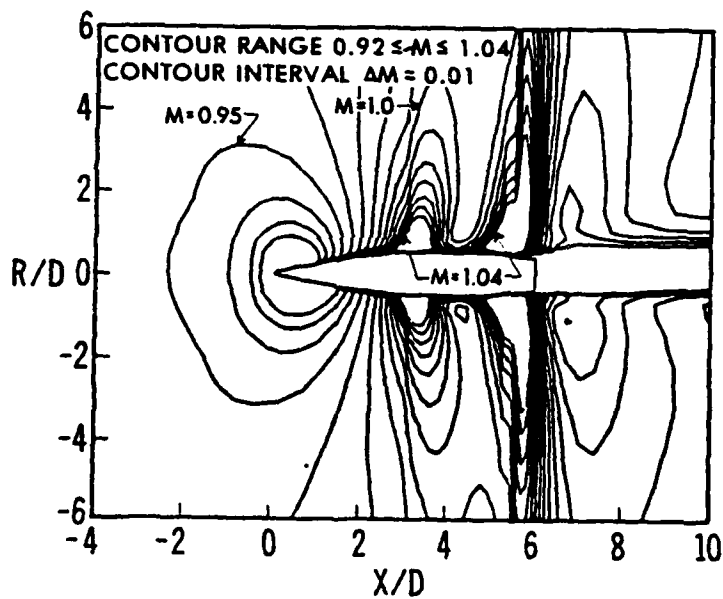


Figure 7. Mach contours for SOCBT, $M = .96$, $\alpha = 2.0^\circ$

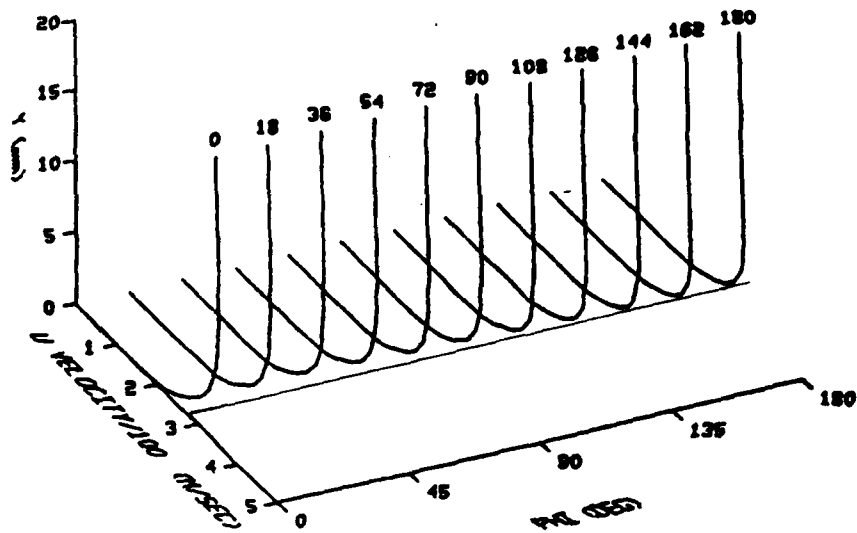


Figure 8a. 3-D velocity profiles, $M = 0.96$, $\alpha = 2.0^\circ$, $X/D = 4.76$

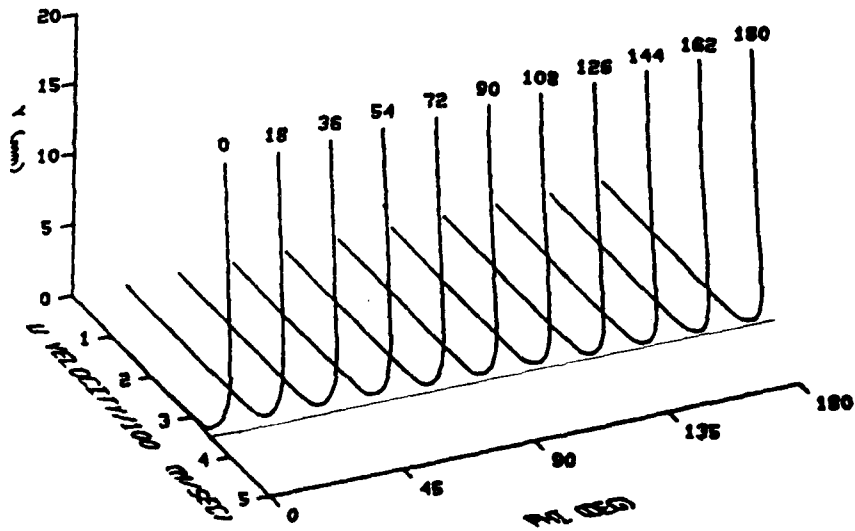


Figure 8b. 3-D velocity profiles, $M = 0.96$, $\alpha = 2.0^\circ$, $X/D = 5.05$

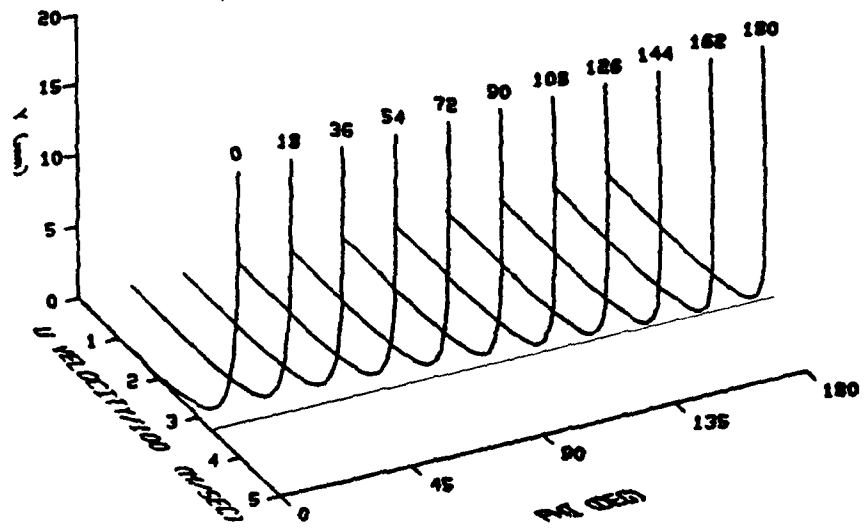


Figure 8c. 3-D velocity profiles, $M = 0.96$, $\alpha = 2.0^\circ$, $X/D = 5.59$

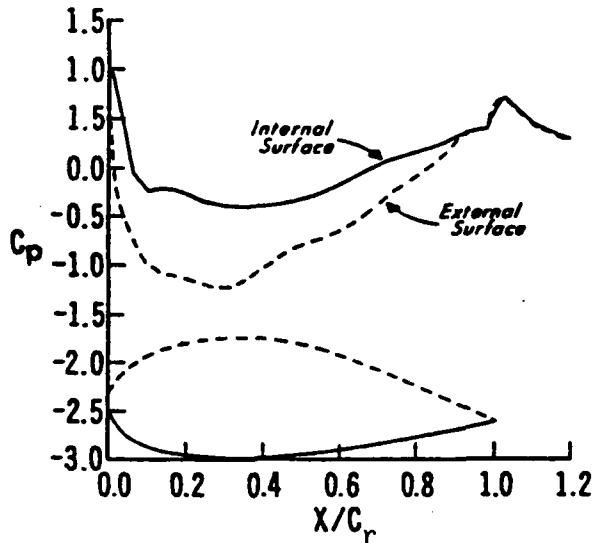


Figure 9a. Inviscid transonic flow over a ring airfoil projectile, $M = 0.4$, $\alpha = 0^\circ$

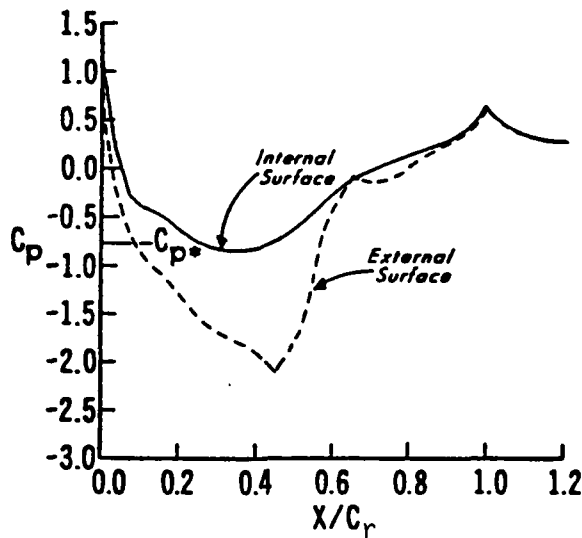


Figure 9b. Inviscid transonic flow over a ring airfoil projectile, $M = 0.7$, $\alpha = 0^\circ$

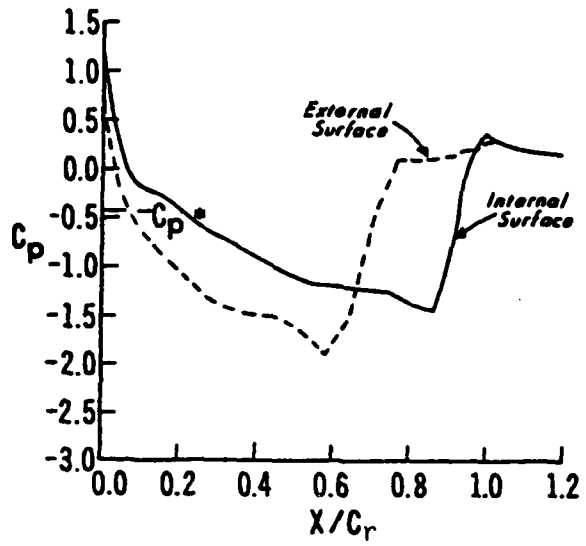


Figure 9c. Inviscid transonic flow over a ring airfoil projectile, $M = 0.8$, $\alpha = 0^\circ$

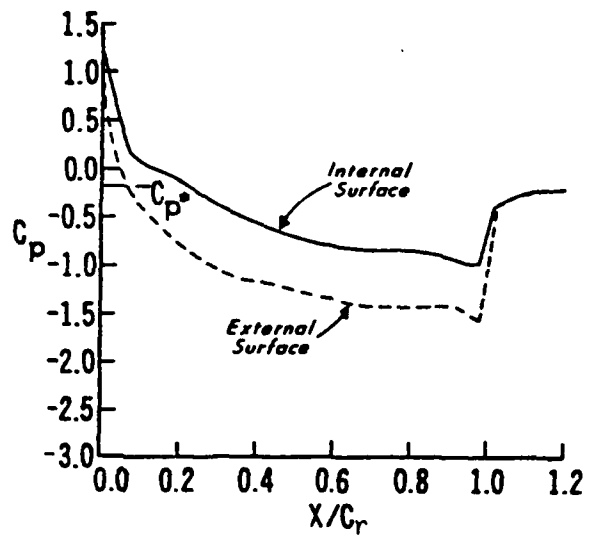


Figure 9d. Inviscid transonic flow over a ring airfoil projectile, $M = 0.9$, $\alpha = 0^\circ$

REFERENCES

1. W. B. Sturek, et al., "Computations of Magnus Effects for a Yawed, Spinning Body of Revolution," AIAA Journal, Vol. 16, No. 7, July 1978, pp. 687-692.
2. L. B. Schiff and W. B. Sturek, "Numerical Simulation of Steady Supersonic Flow Over Cone Ogive-Cylinder-Boattail Body," AIAA Paper No. 80-0066, January 14-16, 1980.
3. R. P. Reklis, W. B. Sturek, and F. L. Bailey, "Computation of Transonic Flow Past Projectiles at Angle of Attack," U.S. Army Ballistic Research Laboratory, ARRADCOM, Technical Report, ARBRL-TR-02139, February 1979. (AD A069106)
4. T. H. Pulliam and J. L. Steger, "On Implicit Finite-Difference Simulations of Three-Dimensional Flow," AIAA Journal, Vol 18, No. 2, February 1980, pp. 159-167.
5. C. J. Nietubicz, T. H. Pulliam, and J. L. Steger, "Numerical Solution of the Azimuthal-Invariant Thin-Layer Navier-Stokes Equations," U.S. Army Ballistic Research Laboratory, ARRADCOM, Technical Report ARBRL-TR-02227, March 1980. AD A085716.
6. J. L. Steger, "Implicit Finite Difference Simulation of Flow About Arbitrary Geometries with Application to Airfoils," AIAA Paper No. 77-665, June 1977.
7. B. S. Baldwin and H. Lomax, "Thin Layer Approximation and Algebraic Model for Separated Turbulent Flows," AIAA Paper No. 78-257, January 1978.
8. R. Beam and R. F. Warming, "An Implicit Factored Scheme for the Compressible Navier-Stokes Equations," AIAA Paper No. 77-645, June 1977.
9. L. D. Kayser, and Whiton, F., "Surface Pressure Measurements on a Boattailed Projectile Shape at Transonic Speeds," BRL-MR. to be published.
10. J. Danberg, Wind tunnel data, to be published as a University of Delaware Report (Private communications).

LIST OF SYMBOLS

a	- speed of sound
C	- proportional constant (see Equation 5)
C_p	- pressure coefficient, $(p-p_\infty)/\frac{1}{2}\rho_\infty a_\infty^2$
c_p	- specific heat (at constant pressure)
C_r	- cord length (see Figure 9)
D	- body diameter (57.15mm)
e	- total energy per unit volume/ $\rho_\infty a_\infty^2$
$\hat{E}, \hat{F}, \hat{G}, \hat{H}, \hat{S}, \hat{q}$	- flux vector of transformed Navier-Stokes equations
J	- transformation Jacobian
M	- Mach number
p	- pressure/ $\rho_\infty a_\infty^2$
Pr	- Prandtl number, $\mu_\infty c_p / \kappa_\infty$
R	- body radius
Re_η	- Reynolds number $\rho_\infty DU_\infty / \mu_\infty$
Re	- Reynolds number, Re_η / M_∞
t	- physical time
u, v, w	- Cartesian velocity components/ a_∞
U, V, W	- Contravariant velocity components/ a_∞
x, y, z	- physical Cartesian coordinates
α	- angle of attack
γ	- ratio of specific heats
κ	- coefficient of thermal conductivity
μ	- coefficient of viscosity

LIST OF SYMBOLS
(Continued)

- ξ, η, ζ - transformation coordinates in axial, circumferential and radial directions
- ρ - density/ ρ_∞
- τ - transformed time
- ϕ - circumferential angle
- Superscript:
- *
- critical value
- Subscript:
- ∞ - free stream conditions

DISTRIBUTION LIST

<u>No. of Copies</u>	<u>Organization</u>	<u>No. of Copies</u>	<u>Organization</u>
12	Administrator Defense Technical Info Center ATTN: DTIC-DDA Cameron Station Alexandria, VA 22314	1	Director US Army Air Mobility Research and Development Laboratory Ames Research Center Moffett Field, CA 94035
1	Commander US Army Materiel Development and Readiness Command ATTN: DRCDMD-ST 5001 Eisenhower Avenue Alexandria, VA 22333	1	Commander US Army Communications Research and Development Command ATTN: DRDCO-PPA-SA Fort Monmouth, NJ 07703
8	Commander US Army Armament Research and Development Command ATTN: DRDAR-TDC DRDAR-TSS (2 cys) DRDAR-LCA-F Mr. D. Mertz Mr. A. Loeb Mr. S. Wasserman Mr. H. Hudgins Mr. E. Friedman Dover, NJ 07801	1	Commander US Army Electronics Research and Development Command Technical Support Activity ATTN: DELSD-L Fort Monmouth, NJ 07703
1	Commander US Army Armament Materiel Readiness Command ATTN: DRSAR-LEP-L, Tech Lib Rock Island, IL 61299	3	Commander US Army Missile Command ATTN: DRSMI-R DRDMI-YDL DRSMI-RDK Mr. R. Deep Redstone Arsenal, AL 35898
1	Director US Army Armament Research and Development Command Benet Weapons Laboratory ATTN: DRDAR-LCB-TL Watervliet, NY 12189	1	Commander US Army Tank Automotive Research and Development Command ATTN: DRDTA-UL Warren, MI 48090
1	Commander US Army Aviation Research and Development Command ATTN: DRDAV-E 4300 Goodfellow Blvd. St. Louis, MO 63120	1	Director US Army TRADOC Systems Analysis Activity ATTN: ATAA-SL, Tech Lib White Sands Missile Range, NM 88002

DISTRIBUTION LIST

<u>No. of Copies</u>	<u>Organization</u>	<u>No. of Copies</u>	<u>Organization</u>
1	Commander US Army Research Office P. O. Box 12211 Research Triangle Park NC 27709	3	Director NASA Ames Research Center ATTN: MS-202A-14 Dr. P. Kutler MS-202-1, Dr. T. Pulliam MS-227-8, Dr. L. Schiff Moffett Field, CA 94035
1	Commander US Naval Air Systems Command ATTN: AIR-504 Washington, D. C. 20360	2	Sandia Laboratories ATTN: Division No. 1331, Mr. H.R. Vaughn Mr. G.R. Eisler P.O. Box 580 Albuquerque, NM 87184
4	Commander US Naval Surface Weapons Center ATTN: Dr. T. Clare, Code DK20 Dr. P. Daniels Mr. D. A. Jones III Mr. L. Mason Dahlgren, VA 22448	1	Stanford University Department of Aeronautics and Astronautics ATTN: Prof. J. Steger Stanford, CA 94035
3	Commander US Naval Surface Weapons Center ATTN: Code 312 Dr. C. Hsieh Dr. W. Yanta Mr. R. Voisinet Silver Spring, MD 20910	1	University of California, Davis Department of Mechanical Engineering ATTN: Prof. H.A. Dwyer Davis, CA 95616
1	Commander US Naval Weapons Center ATTN: Code 3431, Tech Lib China Lake, CA 93555	1	University of Colorado Department of Aerospace Engineering Sciences ATTN: Prof. G. Inger Boulder, CO 80309
1	Director NASA Langley Research Center ATTN: NS-185, Tech Lib Langley Station Hampton, VA 23365	1	University of Delaware Mechanical and Aerospace Engineering Department ATTN: Dr. J. E. Danberg Newark, DE 19711

DISTRIBUTION LIST

<u>No. of Copies</u>	<u>Organization</u>
1	Mr. John Benek MS 600 Calspan Field Services AAFS, TN 37389

Aberdeen Proving Ground

Dir, USAMSAA
ATTN: DRXS-D
DRXS-MP, H. Cohen

Cdr, USATECOM
ATTN: DRSTE-TO-F

Director, USACSL,
Bldg. E3516, EA
ATTN: DRDAR-CLB-PA

USER EVALUATION OF REPORT

Please take a few minutes to answer the questions below; tear out this sheet, fold as indicated, staple or tape closed, and place in the mail. Your comments will provide us with information for improving future reports.

1. BRL Report Number _____

2. Does this report satisfy a need? (Comment on purpose, related project, or other area of interest for which report will be used.)

3. How, specifically, is the report being used? (Information source, design data or procedure, management procedure, source of ideas, etc.) _____

4. Has the information in this report led to any quantitative savings as far as man-hours/contract dollars saved, operating costs avoided, efficiencies achieved, etc.? If so, please elaborate.

5. General Comments (Indicate what you think should be changed to make this report and future reports of this type more responsive to your needs, more usable, improve readability, etc.) _____

6. If you would like to be contacted by the personnel who prepared this report to raise specific questions or discuss the topic, please fill in the following information.

Name: _____

Telephone Number: _____

Organization Address: _____

FOLD HERE

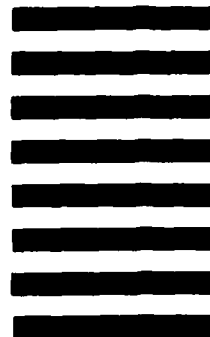
Director
US Army Ballistic Research Laboratory
Aberdeen Proving Ground, MD 21005



NO POSTAGE
NECESSARY
IF MAILED
IN THE
UNITED STATES

OFFICIAL BUSINESS
PENALTY FOR PRIVATE USE, \$300

BUSINESS REPLY MAIL
FIRST CLASS PERMIT NO 12062 WASHINGTON, DC
POSTAGE WILL BE PAID BY DEPARTMENT OF THE ARMY



Director
US Army Ballistic Research Laboratory
ATTN: DRDAR-TSB
Aberdeen Proving Ground, MD 21005

FOLD HERE